Rb deposition on $TiSe_2$ and $TiTe_2$ at 100 K and at room temperature studied by photoelectron spectroscopy

S. E. Stoltz and H. I. Starnberg*
Department of Physics, Göteborg University and Chalmers University of Technology, SE-412 96 Göteborg, Sweden

L. J. Holleboom
Department of Computer Science, Karlstad University, SE-651 88 Karlstad, Sweden
(Received 27 April 2004; revised manuscript received 11 October 2004; published 10 March 2005)

The adsorption of Rb on $TiSe_2$ and $TiTe_2$ at 100 K was studied by high-resolution core level spectroscopy and low energy electron diffraction. At low coverage, Rb formed a dispersed phase, which condensed into a metallic phase as more Rb was deposited. Continued deposition resulted in layer-by-layer growth of Rb, which was particularly conspicuous on $TiTe_2$. Most of the Rb intercalated rapidly as the samples were allowed to warm up. For $TiTe_2$, a small amount of intercalated Rb was detected already at 100 K. When room temperature was reached, only a small fraction of Rb remained on the surface. Equivalent results were obtained instantly when Rb was deposited at room temperature, and valence band spectra from these samples were in excellent agreement with band structures calculated by the linearized augmented plane wave method.

DOI: 10.1103/PhysRevB.71.125403 PACS number(s): 79.60.Bm, 71.20.Tx, 81.15.Ef

I. INTRODUCTION

Layered transition metals dichalcogenides (TMDC's) are a group of highly anisotropic materials, which have been studied extensively during the recent decades.[1–4] They have primarily been used as model systems for studies of a wide range of interesting phenomena associated with their reduced dimensionality, such as charge density wave transitions and enhanced correlation effects. Depending on the valence band filling, they can be either metallic or semiconducting. The formula unit is TX_2 where T is a transition metal (e.g., Ti) and X stands for S, Se, or Te. Each layer consists of a hexagonal sheet of transition metal atoms, sandwiched between two hexagonal chalcogen sheets. The internal bonds in the layers are strong and of mixed ionic and covalent character, while the bonds between adjacent layers are weak and mainly of van der Waals character. Due to this highly anisotropic bonding, one may obtain clean and extremely flat surfaces of high quality by cleavage *in vacuo*, which is a significant experimental advantage. The weakness of the interlayer bond also makes it possible to modify the electronic structure by *in situ* intercalation with, e.g., alkali metals. Intercalation increases the distance between the layers, which implies a more pronounced two-dimensional (2D) character of the electronic structure. The crystallographic structures of these compounds together with the hypothetical $RbTiSe_2$ and $RbTiTe_2$ are shown in Fig. 1. At room temperature, we have already found that Rb which is deposited on $TiTe_2$ at moderate rates under clean conditions intercalates.[5]

It has been reported that Rb deposition on many TMDC surfaces, among them $TiTe_2$, may lead to Rb nanowire formation,[6] and that the Rb deposited on $TiTe_2$ remains in and immediately below the nanowires, without further intercalation.[7] Since the latter claim is contrary to both the results obtained from other alkali metal/TMDC systems and to our previous study, there is a need to further explore the intercalation of alkali metals with TMDC surfaces.

If the alkali metal deposition occur at low temperatures the alkali metals tend to remain on the surface.[8] This opens the possibility to study alkali metal adsorption on TMDC surfaces in more detail. In particular it is of interest to determine different states of adsorbed alkali metals during various stages of overlayer growth, and to study the onset of intercalation as the temperature is raised. Studies of alkali metal deposition on graphite at low temperature has revealed surprisingly complex behavior,[9–15] which provides further motivation for studies of the related alkali/TMDC systems.

We have studied Rb deposition on $TiSe_2$ and $TiTe_2$ with photoelectron spectroscopy and low energy electron diffraction (LEED), at 100 K and at room temperature. We used mainly core level spectroscopy for monitoring of the low temperature adsorption and to study the onset of intercalation as the temperature was raised. In addition we used valence band spectroscopy for accurate band mapping before and after room temperature deposition.

II. EXPERIMENTAL DETAILS

A. Rb deposition at low temperature

The photoelectron spectra were measured at beamline I311 at the MAX-lab synchrotron radiation facility in Lund,

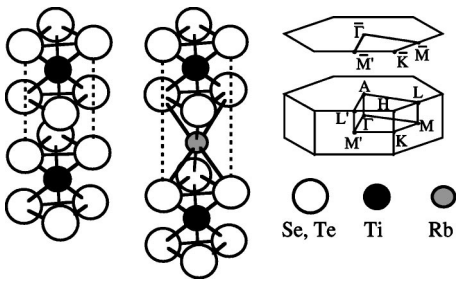

FIG. 1. The crystallographic structures of $TiSe_2$ and $TiTe_2$ together with the hypothetical $RbTiSe_2$ and $RbTiTe_2$ structures. The corresponding surface and bulk Brillouin zones are shown to the left.

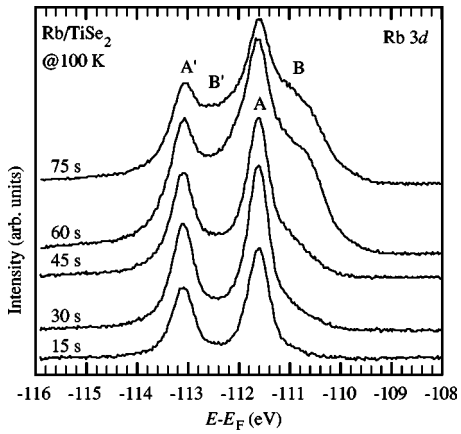

FIG. 2. Normal emission Rb 3*d* spectra measured after 15, 30, 45, 60, and 75 s of Rb deposition on $TiSe_2$. The photon energy was 250 eV.

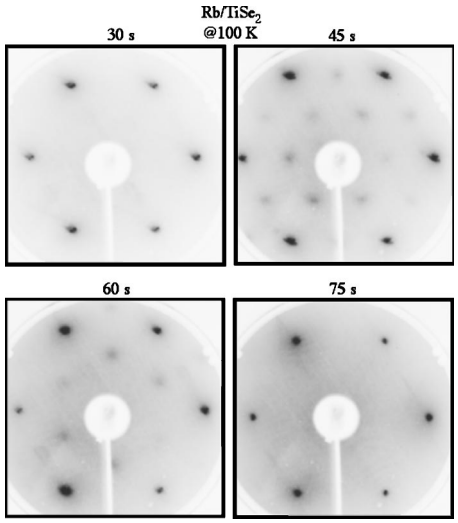

FIG. 3. LEED patterns after Rb deposition on $TiSe_2$. Deposition times are indicated in the figure. After 45 and 60 s of Rb deposition time, 2×2 and $\sqrt{3}\times\sqrt{3}$ superstructures are found. Corresponding photoemission spectra are shown in Fig. 2.

Sweden. This beamline, which includes a modified SX-700 plane grating monochromator and a Scienta 200 electron-energy analyzer, is well suited for high-resolution electron spectroscopy at high photon energies (up to 1500 eV).

The $TiSe_2$ and $TiTe_2$ single crystals were attached to the sample holder by silver filled epoxy resin, and a clean mirrorlike (0001) surface was obtained by cleavage *in vacuo*. The Fermi level cutoff was measured directly from each sample, and all binding energies are given relative to the Fermi level. The sample manipulator included a liquid nitrogen cooling stage, by which the sample could be cooled to 100 K. Rb was deposited *in situ* onto the cold sample from a carefully outgassed SAES getter source, operated at a current of 4.5 A. The Rb emission from this source had an onset about one minute after it was switched on, and stabilized quickly at approximately one monolayer per minute. In the following we generally specify effective deposition times, obtained by subtracting 60 s from the time the source was switched on. The accuracy of this notion was confirmed by the observation that four depositions of effectively 15 s each, produced almost identical results as one deposition of effectively 60 s. At the end of each experimental run, the cooling stage was emptied, and spectra were measured repeatedly as the sample was warming up to room temperature.

The background pressure in the UHV system was in the 10^{-11} torr range during the low temperature experimental runs. Considering the reactivity of the metallic Rb overlayers, and that the measurements extended over several hours, is inevitable that some contamination should occur. This was monitored by frequent recording of valence band spectra, in which contaminants such as O_2, CO, and H_2O are revealed by the appearence of broad nondispersive peaks at ~6 eV binding energy. However, none of our valence band spectra exhibited significant contamination peaks, and additional C 1*s* and O 1*s* core level spectra confirmed that only traces of contaminants were present.

B. Rb deposition at room temperature

All measurements in our angle-resolved study of Rb deposited on $TiSe_2$ and $TiTe_2$ at room temperature were performed at beamline 33 at MAX-lab. The synchrotron radiation was incident at an angle of 45° and polarized in the plane of incidence. The pressure in the UHV system was in the 10^{-10} torr range during the experiment (Rb deposition included). The overall energy resolution was typically ~0.1 eV.

The samples were prepared by cleavage, and were azimuthally oriented by LEED. The position of the Fermi level was determined by measurement from a Ta foil in electrical contact with the sample. All binding energies are given relative to the Fermi level. Rb was deposited *in situ* from a carefully outgassed SAES getter source, operated at a current of 5.5 A. The total effective deposition times (obtained by subtracting 60 s warm-up time from each deposition cycle) were 120 s for $TeSe_2$ and 60 s for $TiTe_2$. In both cases, the depositions were made stepwise with measurements in between, to verify that the intercalation-induced changes were fully developed.

III. RESULTS AND DISCUSSION

A. Low temperature

1. *Rb/$TiSe_2$, submonolayer coverages*

Figure 2 shows Rb 3*d* spectra measured after repeated small Rb depositions on $TiSe_2$, while Figure 3 shows corresponding LEED patterns.

For the smallest coverages, the spectra consist of the two symmetric and relatively narrow peaks A and A', corresponding to the spin-orbit split levels $3d_{3/2}$ and $3d_{1/2}$, respectively. The symmetric line shape, implies that this is not emission from a metallic Rb layer. Our interpretation is that the Rb is initially adsorbed on the surface in a dispersed phase, consisting of ions (or strongly polarized atoms) kept apart by electrostatic repulsion. The absence of extra LEED spots indicates that the dispersed Rb phase lacks long-range order at low coverage.

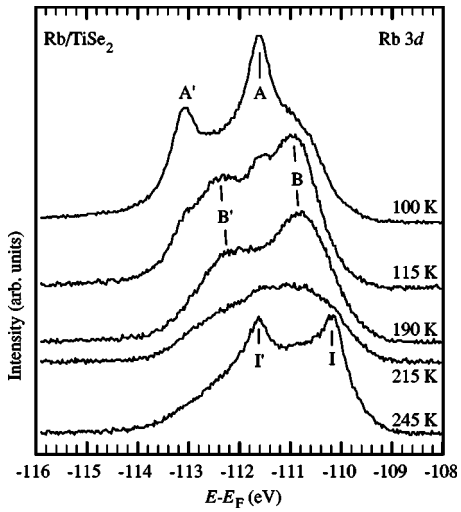

FIG. 4. Normal emission Rb 3*d* spectra measured during warming up from 100 to 245 K after 75 s of Rb deposition on $TiSe_2$. The photon energy was 250 eV.

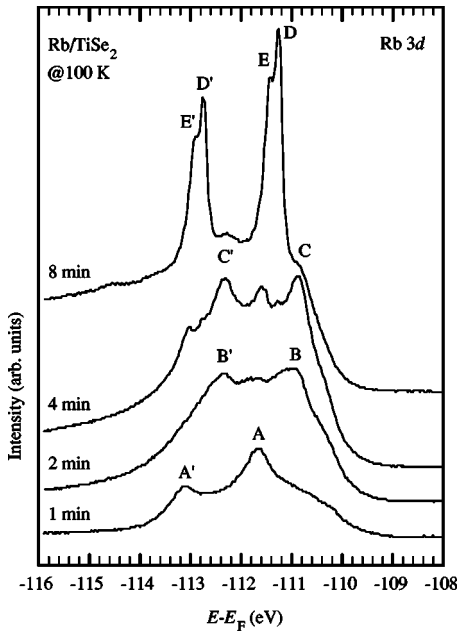

FIG. 5. Normal emission Rb 3*d* spectra measured after 1, 2, 4, and 8 minutes of Rb deposition on $TiSe_2$. The deposition rate was estimated to be ~3Å/min (see Sec. III A 5). The photon energy was 250 eV.

The peaks *A* and *A′* increases somewhat as more Rb is deposited, but more significantly a shoulder *B*, with lower binding energy than *A*, appears. In analogy with the *A*-*A′* pair, the shoulder *B* has also a spin-orbit replica *B′*, which is seen merely as a filling of the valley between *A* and *A′*. We believe that *B* and *B′* represent Rb atoms condensing into metallic islands, co-existing with the dispersed phase between these islands. The *A*-to-*B* ratio was the same in Rb 3*d* spectra recorded at grazing emission angles (θ=75°), which rules out the possibility that one species is on top of the other.

As seen in Fig. 3, the LEED pattern exhibited diffuse 2×2 and $\sqrt{3}\times\sqrt{3}$ superstructures after 45 and 60 s effective deposition times, respectively. The corresponding Rb 3*d* spectra in Fig. 2 indicate mixed surface compositions in both cases, and also after 75 s of Rb deposition, when there is no LEED superstructure at all. Our tentative explanation of this behavior is that the dispersed phase of Rb, at certain densities, forms ordered overlayers which are commensurate with the periodicity of the TMDC substrate. The 2×2 and $\sqrt{3}\times\sqrt{3}$ arrangements of Rb atoms on the $TiSe_2$ surface correspond to nearest-neighbor Rb separations of 7.08 and 6.13 Å, respectively. The nearest-neighbor separation in bulk Rb metal is 4.87 Å, and this value may be a reasonable estimate also for the metallic islands. The persistence of the dispersed phase, although gradually denser, throughout the series of depositions indicates that the deposited amount of Rb is somewhat below a full monolayer even after 75 s of deposition.

Figure 4 shows Rb 3*d* spectra measured while the sample was allowed to warm up. The last spectrum in Fig. 4 was measured 2.5 h after the first one. The peaks *A* and *A′* quickly lost most of their intensity to peaks *B* and *B′*, which became dominant over a large range of temperature. This suggests that the condensed phase of Rb is stable at low temperature, and that the dispersed phase survived below 100 K mainly because of the surface diffusion being slow here. The next major change occurred around 200 K, where peaks *B* and *B′* began losing intensity and were gradually replaced by the spin-orbit doublet *I* and *I′*. Their small widths and lower binding energies are characteristic of intercalated Rb, and considering the damping caused by the $TiSe_2$ layer on top, we conclude that most of the deposited Rb had intercalated before 245 K was reached.

2. Rb/$TiSe_2$, multilayer coverages

Figure 5 shows Rb 3*d* spectra obtained after larger Rb depositions, while Fig. 6 shows corresponding LEED pat-

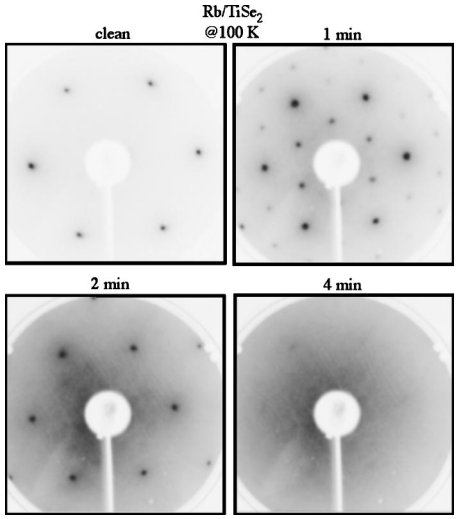

FIG. 6. LEED patterns from the clean $TiSe_2$ crystal, and after Rb deposition. Deposition times are indicated in the figure. A clear $\sqrt{3}\times\sqrt{3}$ superstructure is found after 1 min of Rb deposition. Corresponding photoemission spectra are shown in Fig. 5.

terns. The spectrum at the bottom in Fig. 5 was obtained after one deposition of effectively 1 min, and it is reassuring that it is almost identical to the one obtained after four depositions of effectively 15 s in Fig. 2. As seen in Fig. 6, the $\sqrt{3}\times\sqrt{3}$ LEED superstructure is obtained again, but is sharper than the corresponding pattern in Fig. 3. A likely explanation of the difference is that the single large deposition produced precisely the Rb density needed to obtain a commensurate overlayer, while the repeated small depositions produced a Rb density slightly off the ideal value, with less perfect ordering as a result.

The condensed metallic phase of Rb became dominant after 2 minutes of depositions, as evident from the growth of peak *B* in Fig. 5. Continued Rb depositions will eventually result in metallic multilayers. Then there will be three types of Rb layers which may have distinctly different 3*d* binding energies:

(1) a layer with $TiSe_2$ below and Rb above (interface layer);

(2) layers with Rb on both sides (bulk layers); and

(3) a top layer with Rb below and nothing above (surface layer).

The Rb 3*d* spectra obtained after 4 and 8 min of deposition (see Fig. 5) have three distinct components (apart from the $3d_{1/2}$ replicas), which are labelled *C*, *D*, and *E*. A consistent interpretation is obtained if peak *C* is attributed to the interface layer, peak *D* to bulk layers, and peak *E* to the surface layer. The spectrum obtained after 4 min of deposition is dominated by peaks *C* (interface layer) and *E* (surface layer), while peak *D* (bulk layers) is very weak. This indicates that two layers of Rb are completed, with a third layer just beginning to form. Consequently, 8 min of deposition should correspond to somewhat more than four layers of Rb, and the corresponding spectrum is similar to spectra obtained from bulk Rb.[16]

The spectrum measured after 2 min of deposition should correspond to slightly more than one completed metallic Rb layer. The rather blunt appearance of peak *B* can then be partially understood as due to overlap with the emerging peaks *C* and *E*. It should be noted that a single Rb layer is simultaneously an interface layer and a surface layer, so that peak *B* is fundamentally different from peak *C*, despite being close in binding energy.

As seen in Fig. 6, the LEED pattern vanished completely already after 4 min of Rb deposition. This shows that the Rb multilayers are complete, without holes, and that they lack long-range order.

Figure 7 shows a series of Rb 3*d* spectra measured as the sample with multilayer coverage (obtained by 8 min Rb deposition) was warmed up. The last spectrum in the figure was measured 4 h after the first one. Again the final result is intercalation, but the chain of events is significantly more complex than for the submonolayer case. Initially, there is a drastic loss of intensity for peaks *D* and *E*, and the line shape becomes a broad hump with peaks *C*, *D*, and *E* visible only as small wiggles. The shoulder corresponding to peak *C* persists even at 145 K, but at 155 K all three multilayer peaks have been replaced by a new broader peak F of higher binding energy. At the same time one can also see the first signs of intercalation, as a shoulder corresponding to peak *I* appears. We tentatively attribute the spectral changes to a phase transition, going from a polycrystalline overlayer to a liquid-like overlayer characterized by the broad peak *F*. The liquid-like overlayer is rapidly consumed by intercalation, however, and at 160 K peak *F* is no longer visible. Instead peak *I* has increased drastically, and a new peak *S* emerges with similar binding energy as peak *B* in the submonolayer case. As the temperature increases further, peak *S* is weakened and peak *I* becomes dominant, indicating that the most Rb has intercalated. Finally, also peak *I* has lost intensity, indicating that the Rb intercalated deeper into the substrate. The line shape suggests that a contribution from peak *S* is still present in the end, corresponding to a small amount of condensed Rb remaining on the surface, possibly trapped by impurities, cracks and other defects. This is essentially the same final result as in the submonolayer case, except that the spectral intensities are higher here due to the larger amounts of Rb present.

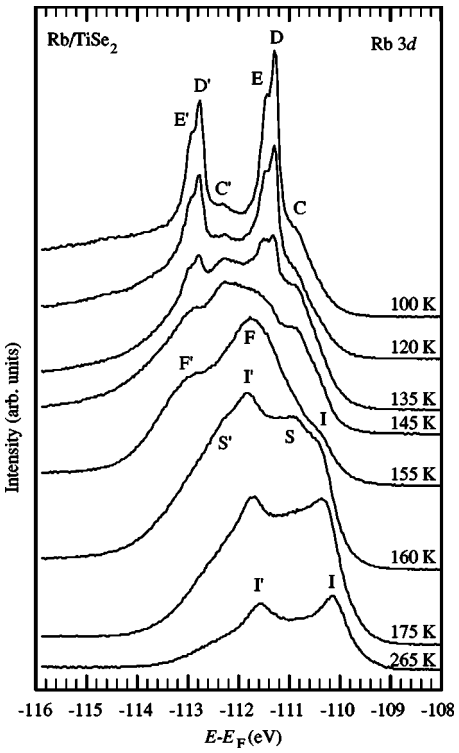

FIG. 7. Normal emission Rb 3*d* spectra measured during warming up from 100 to 265 K after 8 min of Rb deposition on $TiSe_2$. At ~160 K peaks which are characteristic of intercalated Rb appears. The photon energy was 250 eV.

3. Rb/TiTe$_2$

Figure 8 shows Rb 3*d* spectra measured after deposition of various amounts of Rb on $TiTe_2$. Effective deposition times are given for each spectrum. The spectra with 1–5 min deposition times were obtained from the same sample after repeated depositions, each of 1 min effective duration. The spectrum with 50 s deposition time was measured from a different sample. The Rb 3*d* peaks obtained after deposition on $TiTe_2$ are completely analogous to those obtained with $TiSe_2$ as substrate, and they are accordingly labelled in the

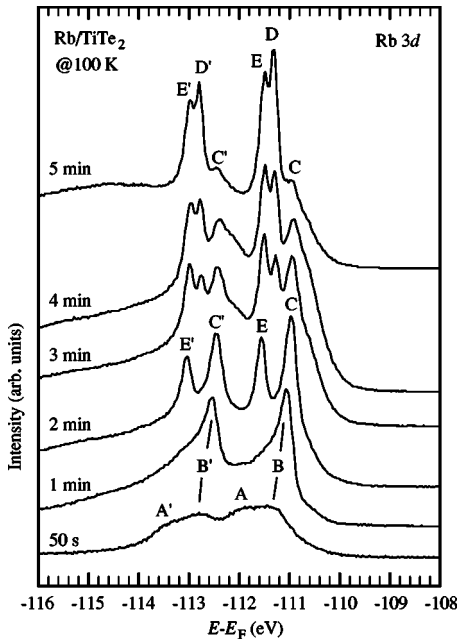

FIG. 8. Normal emission Rb 3*d* spectra measured after 1, 2, 3, 4, and 5 min of Rb deposition on $TiTe_2$. The deposition rate was estimated to be ~5 Å/min (see Sec. III A 5). The photon energy was 250 eV.

same manner. One striking difference, however, is that the spectra corresponding to a few layers of Rb on $TiTe_2$ are much clearer, with very sharp and distinct peaks. It appears that 1 min of deposition time here corresponds closely to one monolayer of Rb. The first Rb monolayer is not complete after 50 s of deposition, and this spectrum shows coexistence of a dispersed phase (peak *A*) and the condensed phase (peak *B*). The corresponding LEED pattern (not shown) has a very weak and diffuse $\sqrt{3}\times\sqrt{3}$ superstructure, which can be attributed to the dispersed phase being accidentally commensurate with the substrate. When the condensed monolayer is complete after one minute of deposition, peak *B* becomes dominant, and in LEED (not shown) each 1×1 spot becomes surrounded by a ring of very weak and diffuse spots. We have no simple explanation for this superstructure, but it could possibly be attributed to a moiré-type interference between the uppermost Te layer and a mismatched close-packed Rb monolayer on top. After 2 min of depositions, peak *B* is replaced by peaks *C* and *E*, as expected for two layers of Rb. The appearance of peak *D* after 3 min of depositions confirms the presence of three Rb layers, each contributing a distinct peak. Adding more layers by continued depositions leads to strengthening of peak *D*, as the number of bulk layers increases, while the interface contribution (peak *C*) is weakened by the increased distance to the surface. The LEED pattern gradually vanished, and no more superstructure was seen. The result after 5 min of depositions on $TiTe_2$ is almost identical to that obtained after 8 min of deposition on $TiSe_2$, which is expected as both cases correspond to polycrystalline Rb multilayer films, thick enough to be rather independent of the substrate.

The Rb 3*d* warming-up sequence for Rb multilayers on $TiTe_2$ is shown in Fig. 9. Peaks *D* and *E* vanishes in the same

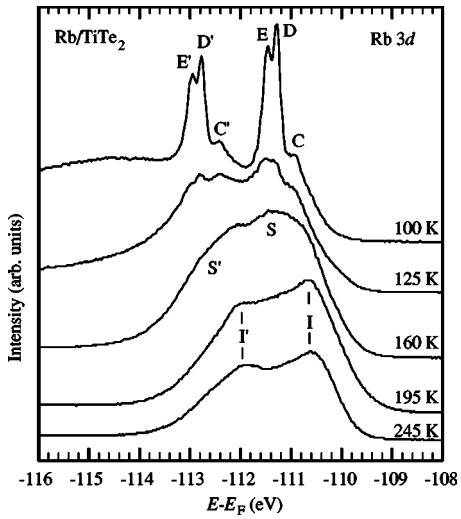

FIG. 9. Normal emission Rb 3*d* spectra measured during warming up from 100 to 245 K after 5 min of Rb deposition on $TiTe_2$. The photon energy was 250 eV.

manner as was seen for the $TiSe_2$ substrate (see Fig. 7), but are not replaced by any peak of the kind we associated with a liquidlike overlayer (peak *F* in Fig. 7). Instead peak *S*, which we attribute to a condensed disordered layer, appears together with the intercalation peak *I*. Possibly the intercalation reaction proceeds so rapidly that there is no time for development of a thicker liquidlike layer in this case. The condensed disordered layer appears more stable but is also continuously losing intensity. The intercalation peak *I* grows as long as there is a rich supply of Rb from the overlayer, but is eventually also losing intensity, which indicates intercalation deeper into the substrate. Again there remains a contribution from surface Rb in the end, although peak S is here only present as a contribution to the asymmetric line shape.

4. Peak fitting of Rb 3d spectra

In order to compare the intercalcation results, we have analyzed Rb 3*d* spectra by peak fitting. Figure 10 shows Rb 3*d* spectra and fitted peaks for the intercalated $Rb/TiSe_2$ and $Rb/TiTe_2$. The spectra were measured from the same samples as those in Figs. 7 and 9, respectively, but not until the temperatures had reached 295 K. The fitting was done using the FitXPS2 peak-fitting software,[17] which employs Doniach-Sunjic profiles[18] convoluted by Gaussians. In both cases adequate fits were obtained using four peaks and a linear background. Binding energies and widths of the fitted peaks are listed in Table I. It is notable that the intercalation peaks *I* and *I′* are much narrower than the surface peaks *S* and *S′*, which reflects the well-defined state of the intercalated Rb. In contrast, the Rb remaining on the surface may occupy sites with more variation in local environment.

It is clear from Table I that the Rb 3*d* binding energy for intercalated Rb is ~0.45 eV higher in $TiTe_2$ than in $TiSe_2$. The chemical shift between adsorbed and intercalated Rb is ~0.57 eV for $TiSe_2$ and ~0.44 eV for $TiTe_2$. These differences may be due to differences in charge transfer and work function, but also the screening in the photoionized state may

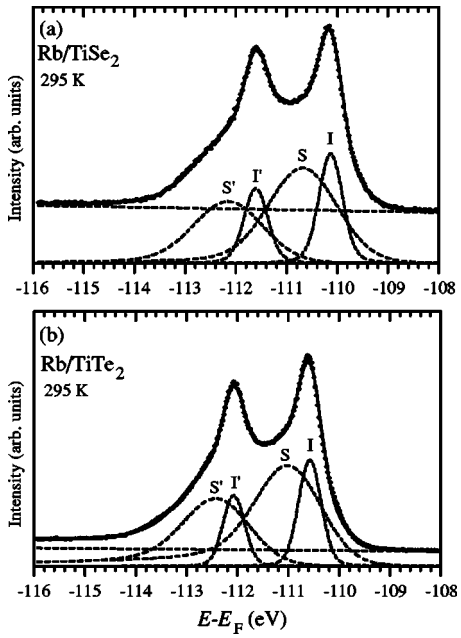

FIG. 10. Normal emission Rb 3*d* spectra measured with a photon energy of 250 eV. The spectra were recorded from (a) $TiSe_2$ and (b) $TiTe_2$, after multilayer Rb deposition at low temperature, followed by warming up to 295 K. Each spectrum was fitted with two spin-orbit doublets and a linear background.

be different for the two substrates. Apart from these small differences, the intercalation reactions of Rb with $TiTe_2$ and $TiSe_2$ seems to be completely analogous.

5. Substrate photoemission

Figure 11 shows Se 3*d* and Te 4*d* spectra measured during multilayer depositions on $TiSe_2$ and $TiTe_2$, respectively. The kinetic energies of the photoelectrons were in the range 60–75 eV in both cases, which means that their mean free paths in metallic Rb should be ~8 Å.[16] The observed decreases of the Se 3*d* and Te 4*d* intensities are therefore expected, and can be used for estimates of the deposition rates. For the $TiSe_2$ case we arrive at a deposition rate of ~3 Å/min (~0.75 ML/min). For the deposition on $TiTe_2$ the rate appears to be significantly higher, ~5 Å/min (~1.2 ML/min). These deposition rates, and in particular the difference, are consistent with the development of Rb 3*d* peaks in Figs. 5 and 8. The lower deposition rate in the $TiSe_2$ case is probably due to decreasing yield of the Rb source, as these measurements were done after the $TiTe_2$ measurements.

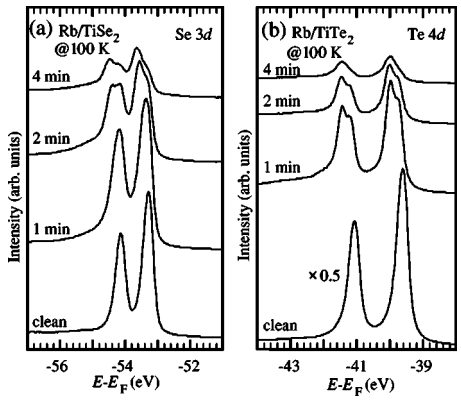

FIG. 11. (a) Normal emission Se 3*d* spectra measured from $TiSe_2$ with a photon energy of 130 eV. (b) Normal emission Te 4*d* spectra measured from $TiTe_2$ with a photon energy of 110 eV. The spectra are recorded from the clean crystals and after 1, 2, and 4 min of Rb deposition.

Apart from the reduced intensities, the most striking effect of Rb deposition seen in Fig. 11 is a conspicuous splitting (~0.3 eV) of the Se 3*d* and Te 4*d* peaks. For both substrates, this splitting becomes visible simultaneously with peak *B* in the Rb 3*d* spectra (see Figs. 5 and 8), and remains visible until the substrate emission is completely suppressed by the Rb overlayer. This suggests that the splitting is induced by the presence of metallic Rb overlayers, and it seems reasonable that one component originates from the uppermost Se or Te layer, which is in direct contact with metallic Rb, while the other component originates from deeper chalcogen layers, which are less affected by the overlayer. We attribute the components of lowest binding energy to the deeper chalcogen layers, since they have lower intensity and are closer in energy to the peaks obtained from clean $TiSe_2$ and $TiTe_2$. The more intense components, with higher binding energy, we accordingly attribute to the uppermost chalcogen layer, but there is clearly a need for theoretical calculations in order to explain why the interaction with the Rb overlayer shifts these components toward higher binding energy.

As the samples warmed up, the Se 3*d* and Te 4*d* intensities increased again, and the splittings vanished. Back at room temperature these spectra exhibited small shifts toward higher binding energies and increased asymmetry, but were otherwise unremarkable, and are consequently not shown here.

TABLE I. Peak energies and full width at half maximum (FWHM) of Rb 3*d* peaks in Fig. 10.

Energy(eV)	*I*	*I′*	*S*	*S′*
$Rb/TiSe_2$	−110.13	−111.61	−110.70	−112.17
$Rb/TiTe_2$	−110.57	−112.07	−111.01	−112.42
FWHM (eV)				
$Rb/TiSe_2$	0.55	0.56	1.62	1.63
$Rb/TiTe_2$	0.53	0.50	1.60	1.60

6. Onset of intercalation

Since intercalation is a thermally activated reaction, it is of primary interest to determine its temperature dependence. A simple analysis of this, based on our warming-up spectra, can be done in two ways.

(1) By monitoring the intensity of substrate emission (i.e., Se 3*d* and Te 4*d* warming-up spectra, which are not shown here), which should increase as the overlayer is consumed by intercalation. The sensitivity of this method depends on the thickness of the deposited layer, however. There is also a possibility that a transformation from uniform overlayers to three-dimensional islands may result in increased substrate emission without any intercalation.

(2) By monitoring the intensity of the intercalation induced peak *I* in Rb 3*d* spectra. The appearance of this peak is an unequivocal indication of intercalation, but again there is a sensitivity problem for thick overlayers. There is also a possibility that a weak intercalation peak is unnoticed if it is overlapped by a close peak of higher intensity.

The rate of a thermally activated reaction is generally proportional to a Boltzmann factor, which means that the onset is gradual as the temperature is increased. We have determined the practical onset temperatures, at which rapid changes were observed in the spectral features induced by intercalation. These onset temperatures are approximate, but are nonetheless useful for prediction of whether significant intercalation will occur or not at a particular temperature.

For the $TiSe_2$ sample with submonolayer Rb coverage, the intensity of Rb 3*d* peak *I* (see Fig. 4) indicated an onset of intercalation at ~230 K. The Se 3*d* intensity was not useful in this case. This is in strong contrast to the $TiSe_2$ sample with multilayer coverage, where both the Rb 3*d* peak *I* intensity (see Fig. 7) and the integrated Se 3*d* intensity showed the onset temperature to be ~160 K. The significantly lower onset temperature in the multilayer case clearly shows that the condensed metallic phase of Rb is more prone to intercalate than the dispersed phase.

The intercalation onset temperature for the $TiTe_2$ sample with multilayer coverage was found to be ~140 K, as judged both from the Rb 3*d* peak *I* intensity (see Fig. 9) and the integrated Te 4*d* intensity. Apparently the activation energy for Rb intercalation is somewhat lower for $TiTe_2$ than for $TiSe_2$. This finding fits in well with the presence of a weak shoulder at ~110.6 eV binding energy in the Rb 3*d* spectra measured during deposition (see Fig. 8). This shoulder coincides in energy with the intercalation peak (see Fig. 9), and is a clear indication that a small amount of Rb intercalated already during the depositions at 100 K. No clear such shoulder was observed during Rb deposition on $TiSe_2$.

7. Comparison with Cs/TiS_2

It is of interest to compare our present results with an earlier study of deposition of Cs on TiS_2 at low temperature.[8] The results are strikingly similar, with Cs forming a dispersed phase, which condensed into a metallic monolayer as the depositions continued. The Cs 4*d* core level then showed a sharp peak analogous with Rb 3*d* peak *B* for the Rb/$TiTe_2$ system (see Fig. 8). The Cs depositions were discontinued at this stage, and instead the sample was allowed to warm up, which led to a meltinglike transition of the condensed layer, subsequently followed by intercalation. It is notable that a small but conspicuous intercalation peak was observed in the Cs 4*d* spectra already during the depositions.

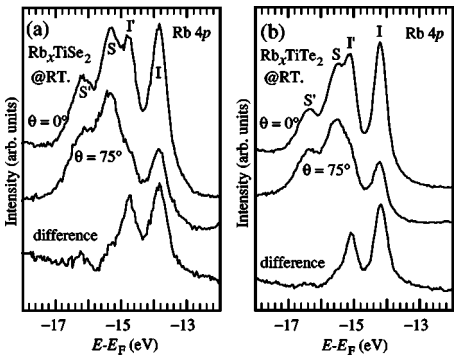

FIG. 12. Rb 4*p* spectra measured from Rb intercalated samples of (a) $TiTe_2$ and (b) $TiTe_2$. The photon energy was 34 eV.

It clearly appears that the three systems Cs/TiS_2, Rb/$TiSe_2$, and Rb/$TiTe_2$ are very similar in terms of adsorption and intercalation. The similarity of Rb and Cs in this context is logical, as these metals are very similar in general terms. It is less expected that the three TMDCs should behave so similarly, however, as they are fundamentally different in terms of their electronic structure. The band structure of TiS_2 consists of six occupied S 3*p* bands, separated from five unoccupied Ti 3*d* bands by a small band gap (~0.2 eV). TiS_2 is therefore a semiconductor, although in practice degenerately *n*-doped by excess Ti.[19,20] $TiTe_2$ has analogous bands of Te 5p and Ti 3*d* character, but instead of a band gap there is an overlap (~0.6 eV), making $TiTe_2$ a semimetal.[21,22] The true nature of $TiSe_2$ has been intensively debated, but recent high-resolution studies point toward a very small band gap (~0.03 eV) at room temperature, and a larger gap (~0.1 eV) at 100 K due to a charge density wave transition with $T_c \approx 200$ K.[23,24] In theory, the presence of a band gap should restrict the transfer of electrons to the substrate, and thus favor the condensation of metallic islands. The observation that alkali metals condenses as readily on metallic $TiTe_2$ as on semiconducting TiS_2 disproves that this mechanism is of importance for the Ti dichalcogenides. It should be noted, however, that all three substrates become metallic as soon as intercalation has begun.

B. Room temperature

1. Core levels

The experiments with deposition of Rb at room temperature were done using a beamline unsuitable for measurement of Rb 3*d* spectra. Instead, we measured the Rb 4*p* core levels, which offer the same kind of information about the chemical state of the Rb. Figure 12 shows Rb 4*p* spectra measured after depositions on (a) $TiSe_2$ and (b) $TiTe_2$. One normal emission spectrum and one spectrum measured at 75° polar emission angle, together with the difference between them, are shown for each substrate. The results are strikingly similar. Four peaks are visible in each spectrum, and in anal-

ogy with the Rb 3*d* results in Sec. III A, we associate the spin-orbit split peaks *I* and *I′* with intercalated Rb and peaks *S* and *S′* with Rb remaining on the surface. The difference spectra show that the principal effect of increased emission angles is an intensity decrease in the *I* and *I′* peaks, thereby confirming that they originate from intercalated Rb. The results obtained after room temperature depositions are essentially the same as those obtained by low temperature depositions followed by warming to room temperature, although the relative intensity of the *S* and *S′* peaks appears to be higher in Fig. 12 than in Fig. 10. Partly this is due to the Rb 4*p* spectra being more surface sensitive (due to lower kinetic energies of the photoelectrons), but it is also possible that more Rb was trapped on the surface by contamination from the Rb sources, which were run at higher current to compensate for the lower sticking coefficient at room temperature. The chemical shifts (~1 eV) between *I* and *S* seen in Fig. 12 are similar to what is found for other alkali/TMDC systems,[25] but larger than those found in Table I. Also this difference may be due to a larger degree of contamination after the room temperature depositions. It should be considered, however, that the *S* and *S′* peak positions in Table I are obtained through peak fitting but not directly observable, and may therefore be less accurate.

The Se 3*d* and Te 4*d* spectra measured after the room temperature depositions (not shown here) exhibited small shifts (~0.1 eV) toward higher binding energies and increased asymmetry (especially Se 3*d*), but were otherwise unremarkable. Compared to Se 3*d* and Te 4*d* spectra obtained after low temperature deposition and subsequent warming, there are no significant differences.

2. Valence bands

Series of angle-resolved valence band spectra were measured in the $\bar{\Gamma}\bar{M}$ and $\bar{\Gamma}\bar{K}\bar{M}$ azimuthal directions, with $h\nu = 20$ eV for $TiSe_2$ and $h\nu = 22$ eV for $TiTe_2$, before and after Rb intercalation. These series of spectra were used to construct structure plots, which show the energies of spectral features plotted against $k_{\|}$ (the surface-parallel component of the photoelectron wave vector). Instead of manual determination of peak positions, we used a procedure based on the second derivative of each spectrum: After Gaussian smoothing [full width at half maximum (FWHM) 0.14 eV] of the second derivative we marked the energy ranges where the second derivative was negative below a certain limit. This limit, and the degree of smoothing, were chosen in order to eliminate noise-induced false peaks, without missing true peaks. As an example, Fig. 13 shows a typical spectrum, its second derivative, and the resulting indication of spectral peaks.

Figure 14 shows the resulting structure plots for $TiSe_2$ and Rb_xTiSe_2, while Fig. 15 shows those for $TiTe_2$ and Rb_xTiTe_2. The peaks are indicated by bars along lines of constant emission angle. A significant advantage of this mode of representation is that not only the positions of the peaks are shown, but also their widths. One should be aware, however, that overlapping peaks may show up as single long bars in the plots.

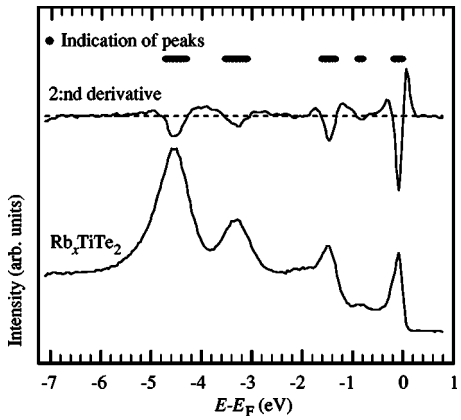

FIG. 13. A valence band spectrum of Rb_xTiTe_2, together with its second derivative is negative. The spectrum was obtained at a polar emission angle of 10° in the $\bar{\Gamma}\bar{M}$ azimuthal direction The photon energy was 22 eV.

In addition to structure plots, Figs. 14 and 15 also contain calculated energy bands along the symmetry lines ΓM, ΓKM, (solid lines) *AL*, and *AHL* (dashed lines). However, as the perpendicular wave vector component is not conserved in the photoemission process, the experimental structure plots should be compared with the surface projected band structures. Close approximations to the surface projected band structures are provided by the cross-hatched areas between connected pairs of bands.

The calculations were self-consistent and scalar-relativistic, but did not include spin-orbit splitting. They were done by the linearized augmented plane wave (LAPW) method, and the parametrized Ceperley-Alder[26] form of the exchange-correlation potential was used. The lattice parameters used in the calculations for $TiSe_2$ were $a = 3.450$ Å (distance between nearest-neighbor atoms within a sheet) and $c = 6.008$ Å (distance between two equivalent atoms in adjacent layers). For the hypothetical $RbTiSe_2$ structure we used $a = 3.540$ Å and $c = 8.058$ Å. For $TiTe_2$ and $RbTiTe_2$ we used $a = 3.778$ Å for both, and $c = 6.493$ Å and 8.382 Å, respectively. The new values of c was estimated from ion radius considerations, using $r = 1.48$ Å for Rb^+.

The calculated bands for $RbTiSe_2$ and $RbTiTe_2$ were shifted upwards by ~0.1 eV, to obtain the best possible agreement with the structure plot. After this energy shift, the agreement between the structure plot and the approximate surface band structure is excellent. The energy shift is justified because the calculations were done for a fully intercalated system, while in reality we had Rb_xTiSe_2 and Rb_xTiTe_2 with $x < 0.5$, and consequently a smaller occupation of the Ti 3*d* band. The surface projected bands are much narrower after Rb intercalation, as a consequence of the decreased perpendicular dispersion, connected with the increased layer separation. Generally, (c) and (d) in Figs. 14 and 15 show an agreement between our experimental structure plots and the calculated band structure, which would be unlikely if the deposited Rb had not intercalated. However, after intercalation, stationary peaks are seen immediately below the Fermi level, even where the Ti 3*d* should be unoccupied, e.g.,

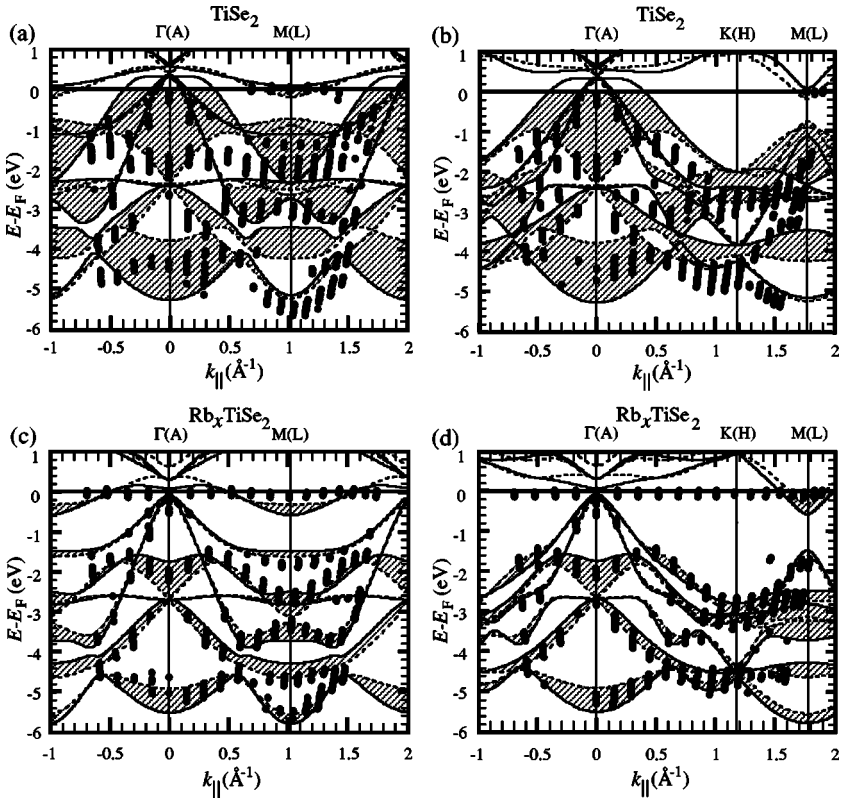

FIG. 14. (a): Structure plot for clean $TiSe_2$ along the $\bar{\Gamma}\bar{M}$ azimuthal direction. Black bars correspond to spectral peaks, which are compared with ΓM (full lines) and *AL* (dashed lines) bands calculated by the LAPW method. The cross-hatched areas approximate the surface projected band structure. The structure plots were obtained from spectra measured with $h\nu$=20 eV. (b) Same as (a), but along the $\bar{\Gamma}\bar{K}\bar{M}$ azimuthal direction. (c) As (a), but the structure plot where obtained from spectra measured after Rb deposition, and they are compared with (energy shifted) calculated bands for the hypothetical $RbTiSe_2$ compound. (d) Same as (c), but along the $\bar{\Gamma}\bar{K}\bar{M}$ azimuthal direction.

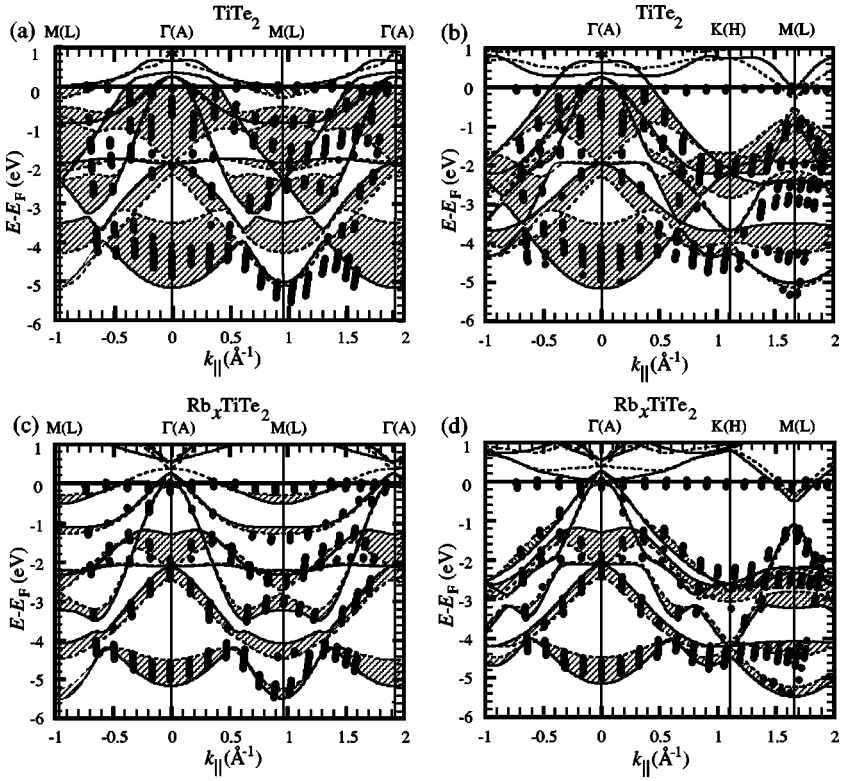

FIG. 15. (a) Structure plot for clean $TiTe_2$ along the $\bar{\Gamma}\bar{M}$ azimuthal direction. Black bars correspond to spectral peaks, which are compared with ΓM (full lines) and *AL* (dashed lines) bands calculated by the LAPW method. The cross-hatched areas approximate the surface projected band structure. The structure plot were obtained from spectra measured with $h\nu$=22 eV. (b) Same as (a), but along the $\bar{\Gamma}\bar{K}\bar{M}$ azimuthal direction. (c) As (a), but the structure plot where obtained from spectra measured after Rb deposition, and they are compared with (energy shifted) calculated bands for the hypothetical $RbTiTe_2$ compound. (d) Same as (c), but along the $\bar{\Gamma}\bar{K}\bar{M}$ azimuthal direction.

around $K(H)$. These peaks are caused by the action of the Fermi cutoff on the tails of the bands above the Fermi level. Inelastic scattering from occupied regions of the Brillouin zone may also contribute to these peaks.

IV. CONCLUSIONS

Rb deposited on $TiSe_2$ and $TiTe_2$ at 100 K is initially adsorbed in a dispersed phase, which gradually becomes denser. This phase lacks long-range order, except at densities where the Rb-Rb distances happen to be commensurate with periodicity of the TMDC surface, which is revealed by weak 2×2 or $\sqrt{3}\times\sqrt{3}$ superstructures in LEED.

When the deposition continued, the dispersed Rb began to condense into metallic islands of monolayer thickness. In the Rb 3*d* spectra, this new phase of adsorbed Rb was distinguished from the dispersed phase by producing peaks of lower binding energy. For submonolayer coverages, both phases were seen to co-exist. After completion of the first metallic monolayer, the Rb films grew in a layer-by-layer fashion, and three different components were seen in the Rb 3*d* spectra, corresponding to the interface layer, bulk layers, and the surface layer, respectively. For the double-layer Rb film, the bulk component was missing. The layer-by-layer growth of Rb was particularly striking on the $TiTe_2$ surface. The behavior of the $Rb/TiSe_2$ and $Rb/TiTe_2$ systems is very similar to that previously found for the Cs/TiS_2 system, despite significant differences in the electronic nature of the different TMDCs.

Upon warming to room temperature, the deposited Rb intercalated into both $TiSe_2$ and $TiTe_2$. The intercalation was evident from the appearance of specific intercalation peaks in the Rb 3*d* spectra, the vanishing of the overlayer peaks, and increased emission from the TMDC layers. For multilayer Rb films, on both TMDCs, the layer-specific sharp peaks in the Rb 3*d* spectra vanished and were replaced by much broader structures, before the onset of massive intercalation. This observation suggests that the Rb films underwent some kind of melting transition. Rapid intercalation was observed when the temperature reached $\sim$160 K for $TiSe_2$ and $\sim$140 K for $TiTe_2$, but in the latter case a small amount of Rb was found intercalated already during deposition, at 100 K. These results indicate a somewhat lower energy barrier for intercalation in $TiTe_2$. For $TiSe_2$ with submonolayer Rb coverage, the onset temperature for intercalation was found to be $\sim$230 K, which is significantly higher than with multilayer coverage.

Warming to room temperature in all cases resulted in Rb 3*d* spectra with sharp intercalation peaks, and broader peaks of higher binding energy, corresponding to Rb trapped on the surface.

Deposition of Rb at room temperature resulted in prompt intercalation, and the Rb 4*p* spectra showed intercalation and surface components, which were clearly identified through their different sensitivities to emission angle changes. Apparently, the final results of room temperature deposition, and deposition at low temperature followed by warming up to room temperature, are the same. The binding energies of surface-related features in the core level spectra may vary, however, depending on the deposition conditions, e.g., total Rb dose and presence of contaminants.

Structure plots constructed from angle-resolved valence band spectra from both pure and Rb intercalated $TiSe_2$ and $TiTe_2$ were found to be in excellent agreement with band structures calculated by the LAPW method. The agreement was particularly striking for the intercalated samples.

We have reached a fairly good understanding of the studied systems, but some vital issues remain to be clarified. One such issue is the nature of the alkali metal remaining on the surface: Is it uniformly distributed or trapped by defects? How is it affected by contamination? Another big question is the importance of defects in the intercalation process. It seems likely that spectroscopy needs to be complemented by other techniques, such as photoelectron microscopy and scanning probe microscopy to address these issues.

ACKNOWLEDGMENTS

This work was financially supported by the Swedish Research Council. The authors also thank the staff at MAX-lab for valuable assistance.

*Electronic address: starn@fy.chalmers.se

[1] J. A. Wilson and A. D. Yoffe, Adv. Phys. **18**, 193 (1969).
[2] *Intercalated Layered Materials*, edited by F. A. Levy (D. Reidel, Dordrecht, 1979).
[3] R. H. Friend and A. D. Yoffe, Adv. Phys. **36**, 1 (1987).
[4] *Electron Spectroscopies Applied to Low-Dimensional Materials*, edited by H. P. Hughes and H. I. Starnberg (Kluwer, Dordrecht, 2000).
[5] S. E. Stoltz, H. I. Starnberg, and L. J. Holleboom, Europhys. Lett. **64**, 816 (2003).
[6] R. Adelung, L. Kipp, J. Brandt, L. Tarcak, M. Traving, C. Kreis, and M. Skibowski, Appl. Phys. Lett. **74**, 3053 (1999).
[7] R. Adelung, J. Brandt, K. Rossnagel, O. Seifarth, L. Kipp, M. Skibowski, C. Ramirez, T. Strasser, and W. Schattke, Phys. Rev. Lett. **86**, 1303 (2001).
[8] H. I. Starnberg, H. E. Brauer, and V. N. Strocov, Surf. Sci. **384**, L785 (1997).
[9] Z. Y. Li, K. M. Hock, and R. E. Palmer, Phys. Rev. Lett. **67**, 1562 (1991).
[10] K. M. Hock and R. E. Palmer, Surf. Sci. **284**, 349 (1993).
[11] J. C. Banard, K. M. Hock, and R. E. Palmer, Surf. Sci. **287/288**, 178 (1993).
[12] M. R. C. Hunt, P. J. Durston, and R. E. Palmer, Surf. Sci. **364**, 266 (1996).
[13] P. Bennich, C. Puglia, P. A. Brühwiler, A. Nilsson, A. J. Maxwell, A. Sandell, N. Mårtensson, and P. Rudolf, Phys. Rev. B **59**, 8292 (1999).
[14] M. Breitholtz, T. Kihlgren, S. Å. Lindgren. and L. Walldén, Phys.

Rev. B **66**, 153401 (2002).
[15] M. Breitholtz, T. Kihlgren, S. Å. Lindgren, and L. Walldén, Phys. Rev. B **67**, 235416 (2003).
[16] G. K. Wertheim, D. M. Riffe, N. V. Smith, and P. H. Citrin, Phys. Rev. B **46**, 1955 (1992).
[17] D. L. Adams, *FitXPS2 peak-fitting software*, University of Aarhus, Denmark, 2001, http://www.sljus.lu.se/download.html
[18] S. Doniach and M. Sunjic, J. Phys. C **3**, 285 (1970).
[19] P. C. Klipstein and R. H. Friend, J. Phys. C **17**, 2713 (1984).
[20] D. R. Allan, A. A. Kelsey, S. J. Clark, R. J. Angel, and G. J. Ackland, Phys. Rev. B **57**, 5106 (1998).
[21] R. Claessen, R. O. Anderson, G.-H. Gweon, J. W. Allen, W. P. Ellis, C. Janowitz, C. G. Olson, Z.-X. Shen, V. Eyert, M. Skibowski, K. Friemelt, E. Bucher, and S. Hüfner, Phys. Rev. B **54**, 2453 (1996).
[22] L. Perfetti, C. Rojas, A. Reginelli, L. Gavioli, H. Berger, G. Margaritondo, M. Grioni, R. Gaál, L. Forró, and F. Rullier Albenque, Phys. Rev. B **64**, 115102 (2001).
[23] K. Rossnagel, L. Kipp, and M. Skibowski, Phys. Rev. B **65**, 235101 (2002).
[24] T. E. Kidd, T. Miller, M. Y. Chou, and T.-C. Chiang, Phys. Rev. Lett. **88**, 226402 (2002).
[25] H. I. Starnberg, H. E. Brauer, and H. P. Hughes, in *Electron Spectroscopies Applied to Low-Dimensional Materials*, edited by H. P. Hughes and H. I. Starnberg (Kluwer, Dordrecht, 2000), p. 41.
[26] D. M. Ceperley and B. J. Alder, Phys. Rev. Lett. **45**, 566 (1980).